The role of streamwise perturbations in pipe flow transition

Fernando Mellibovsky and Alvaro Meseguer

Citation: Phys. Fluids **18**, 074104 (2006); doi: 10.1063/1.2222376
View online: http://dx.doi.org/10.1063/1.2222376
View Table of Contents: http://pof.aip.org/resource/1/PHFLE6/v18/i7
Published by the American Institute of Physics.

The role of streamwise perturbations in pipe flow transition

Fernando Mellibovsky[a] and Alvaro Meseguer[b]
Departament de Física Aplicada, Universität Politècnica de Catalunya, C/Jordi Girona 1-3, Mod. B5, 08034 Barcelona, Spain

(Received 7 November 2005; accepted 21 June 2006; published online 17 July 2006)

The phenomenon of subcritical transition in Hagen-Poiseuille or pipe flow is explored for a wide range of Reynolds numbers within the interval $\mathrm{Re} \in [2.5\times10^3, 1.26\times10^4]$ by means of a computational method that numerically resolves the transitional dynamics with nearly 3.5×10^4 degrees of freedom on a medium aspect-ratio domain of length $32\pi/5$. The aim of this exploration is to provide a theoretical characterization of the basin of attraction of the basic regime by measuring the minimal amplitude of an initial global perturbation leading to transition. The analysis is based on a particular theoretical scenario that considers streamwise-independent finite amplitude initial vortical perturbations that trigger global transition via optimal inflectional instabilities of streamwise-dependent modes with selected axial wave numbers. Disturbances consisting of 1, 2, and 3 pairs of vortices are investigated. Special attention is given to relaminarization phenomena that is frequently observed for low Reynolds numbers. Long lasting turbulent regimes and relaminarized flows are distinguished by means of time integrations of suitable length between $T_{\min}=600$ and $T_{\max}=1000$ advective time units. Some transitional runs are specifically analyzed to exemplify the transition scenario under investigation and its independence of pipe length is verified with a few computations on a longer pipe of length 32π (1.4×10^5 degrees of freedom). For large values of the Reynolds number, a theoretical scaling law for the threshold amplitude of a perturbation required to trigger transition is provided. Different types of perturbations seem to respond to different scaling laws. © *2006 American Institute of Physics*. [DOI: 10.1063/1.2222376]

I. INTRODUCTION

Transition to turbulence in shear flows still remains an open problem of hydrodynamic stability theory. For instance, plane Couette flow (fluid contained between inertially sliding infinite parallel plates) is always linearly stable, i.e., any infinitesimal perturbation of the flow decays for long times, yet it exhibits transition to turbulence in the laboratory and in numerical simulations for moderate flow speeds.[1–4] Hagen-Poiseuille or pipe flow (pressure driven flow through an infinite circular pipe) is believed to be linearly stable as well but also becomes turbulent in practice.[5–9] Plane Couette and pipe flow, because of their apparent simplicity, are the most fundamental examples of *subcritical* transition to turbulence in fluid dynamics, i.e., transition to turbulence bypassing linear stability.

Since the seminal work of Osborne Reynolds[10] published in 1883, many physicists and applied mathematicians have devoted enormous efforts to provide a theoretical explanation of the phenomenon of subcritical transition to turbulence in plane Couette or pipe flows. During the last decade, the pursuit of an answer has followed two independent research approaches. The first one has been mainly focused on the study of nonmodal transient growth exhibited by streamwise vortical finite amplitude perturbations, due to the strong non-normality of the linearized Navier-Stokes operator, i.e., nonorthogonality of its eigenvectors.[7,11–14] This transient growth eventually stagnates, leaving an almost steady modulated streamwise flow that contains two-dimensional *streaks*, characterized by the presence of saddle points, potentially unstable with respect to three-dimensional infinitesimal perturbations in the *inviscid* stage, i.e., before the viscous effects take over the dynamics. Almost exponential growth of streamwise-dependent waves is therefore expected under the presence of streaks, eventually inducing transition via a mechanism commonly termed *streak breakdown*, by which the three-dimensional waves break the streamwise structure of the streaks, leading to turbulence. The described instability process has been proven to be a universal mechanism of subcritical transition in other shear flows such as Blasius boundary layer or plane Poiseuille flow, although other scenarios may also be at work in the transition process.[15,16]

The second approach to the problem of subcritical transition has been based on the direct exploration of the phase map of the corresponding dynamical system representing the fluid problem. Subcritical transition in linearly stable open shear flows is directly related to the existence of secondary solutions of the Navier-Stokes equations. Since these flows are linearly stable for all Reynolds numbers, these other solutions must be necessarily disconnected from the basic flow. For example, in plane Couette flow, secondary solutions were found[17,18] by means of homotopy transformations. More recent numerical studies[4,19] have also reported new solutions for this particular problem. In pipe flow, recent numerical studies have revealed the existence of travelling wave solutions of selected azimuthal symmetry, supposedly

[a]Electronic mail: fmellibovsky@fa.upc.edu
[b]Author to whom correspondence should be addressed. Electronic mail: alvar@fa.upc.edu

constituting the essential topological feature of the chaotic dynamics.[20,21] The limit cycles associated with these travelling waves have been proved to be linearly unstable.[22] The computation of the friction factor associated to these time-dependent solutions ostensibly matches the empirical laws describing turbulent flows in smooth pipes,[20] which in itself constitutes a clear signature of the relevance of these solutions in the turbulent regime.

In Hagen-Poiseuille flow, a fluid of kinematic viscosity ν is axially driven through a circular pipe of radius a by means of a uniform axial pressure gradient. The basic solution of the Navier-Stokes equations is a parabolic, streamwise independent, axisymmetric, and steady purely axial flow. The *Reynolds number* is defined as $\mathrm{Re}=U_{\mathrm{cl}}a/\nu$, where U_{cl} is the maximum axial speed of the flow at the centerline of the pipe. Experimental evidence shows that pipe flow becomes more sensitive to perturbations when increasing the Reynolds number. Since the flow is linearly stable, finite (yet small) amplitude perturbations must be responsible for the transition to turbulence.

One of the main goals of the two previously described approaches to subcritical turbulence has been to provide a characterization of the *basin of attraction* of the basic laminar flow. We must think of it as a subset in an infinite dimensional space that contains the basic flow, driving towards this solution any initial perturbation contained in this subset. Numerical simulations confirm that pipe flow is even stable for *all* axisymmetric finite-amplitude disturbances.[23] Therefore, the basin of attraction *is not* a bounded domain and its *size* is a meaningless measure because it is actually infinite. Instead, we must think of the boundary of that basin of attraction that approaches a minimum amplitude A_c from the steady solution. A question still unsolved is the dependence of this amplitude with the Reynolds number, $A_c=A_c(\mathrm{Re})$, that must necessarily decrease when Re is increased, being plausible to assume that its asymptotic behavior scales with Re according to

$$A_c \sim \mathrm{Re}^{\gamma}, \tag{1}$$

with γ necessarily negative. In other words, A_c represents the minimum amplitude of a perturbation capable of destabilizing the basic profile, leading to a turbulent regime. Theoretical exponents for plane channel flows have been obtained by means of asymptotic methods within the framework of some particular transition scenarios.[16] For pipe flow, recent renormalizations[24] have been suggested in order to cast different experimental results in terms of a single definition of the amplitude appearing in (1), providing lower and upper bounds for the value of this critical exponent that presumably lies within the interval $\gamma \in [-9/5, -6/5]$.

The most comprehensive experimental explorations of the threshold amplitude problem (1) for pipe flow were provided by Darbyshire and Mullin[8] and more recently by Hof, Juel, and Mullin,[9] henceforth referred as HJM, where the fluid was perturbed by means of localized injections of selected azimuthal symmetry. The experimental results of HJM clearly concluded that the minimum amplitude of a perturbation required to trigger transition scaled as the inverse of the Reynolds number, i.e., $A_c=\mathcal{O}(\mathrm{Re}^{-1})$. Postprocessed experimental results have recently confirmed the presence of the aforementioned travelling waves obtained computationally[20,21] as inherent components of the turbulent flow.[25]

To the authors' knowledge, the first computational estimation of the threshold exponent problem (1) in pipe flow was provided by Meseguer,[12] employing a numerical model for time integrations that were too short in time, thus being impossible to distinguish between relaminarized and turbulent flows, particularly for low Re. The resolution was extremely poor, especially in the axial direction, for which a singe mode was considered, not allowing for nonlinear interaction. By contrast, the present study provides a highly resolved comprehensive numerical exploration of the threshold amplitude for $2.5\times10^3<\mathrm{Re}<1.26\times10^4$, based on the streak breakdown scenario, for medium length pipe aspect ratio and for extended time horizons that allow us to distinguish between long-lasting turbulence and relaminarization. Streamwise perturbations consisting of a varying number of pairs of vortices are used as initial disturbances, optimal streamwise-dependent waves and random noise are alternatively added as the 3D component of the perturbation, the development of the flow is carefully analyzed for some test cases and the independence of the considered transition scenario with respect to pipe length suitably verified.

The paper is structured as follows: Sec. II is devoted to the mathematical formulation of the initial value problem for the perturbation fields, and the axial and azimuthal structure of disturbances is presented. The criteria that allow us to classify laminar, relaminarized and turbulent flows are explained in Sec. III, where the time horizons required to distinguish among those regimes are provided. Section IV yields the main results of the exploration for different types of streamwise disturbances and also investigates the effects of pipe length in this particular transition scenario. Finally, many questions regarding the difficulties of comparing numerics with recent experimental results are addressed. The main conclusions are gathered and presented in Sec. V.

II. THE INITIAL VALUE PROBLEM

In cylindrical nondimensional coordinates (r,θ,z), the basic Hagen-Poiseuille flow reads $\mathbf{u}_b=u_b\hat{\mathbf{r}}+v_b\hat{\boldsymbol{\theta}}+w_b\hat{\mathbf{z}}=(1-r^2)\hat{\mathbf{z}}=(0,0,1-r^2)$, where we have used a and $\mathrm{U_{cl}}$ as units for space and velocity, respectively. The computational domain considered is $(r,\theta,z)\in\mathfrak{D}=[0,1]\times[0,2\pi]\times[0,\Lambda]$, where the dimensionless pipe length in radii units is fixed to $\Lambda=6.4\pi\sim20$ (except for a subset of runs on a much longer pipe, with $\Lambda=32\pi\sim100$, carried out for verification purposes). The total flow is decomposed into the basic flow $\mathbf{u}_b$ plus a time-dependent solenoidal disturbance $\mathbf{u}(r,\theta,z,t)$, satisfying radial homogeneous boundary conditions, $\mathbf{u}(1,\theta,z,t)=0$, and axial-azimuthal periodicity,

$$\mathbf{u}(r,\theta+2\pi,z,t)=\mathbf{u}(r,\theta,z+\Lambda,t)=\mathbf{u}(r,\theta,z,t). \tag{2}$$

Formal substitution of the perturbed field $\mathbf{v}=\mathbf{u}_b+\mathbf{u}$ in the Navier-Stokes equations, leads to a nonlinear partial differential equation for the perturbation of the form

$$\partial_t \mathbf{u} = \frac{1}{\mathrm{Re}}\Delta\mathbf{u} - (\mathbf{u}_b \cdot \nabla)\mathbf{u} - (\mathbf{u} \cdot \nabla)\mathbf{u}_b - (\mathbf{u} \cdot \nabla)\mathbf{u}, \tag{3}$$

with

$$\nabla \cdot \mathbf{u} = 0. \tag{4}$$

Equation (3) is discretized by means of a solenoidal spectral Petrov-Galerkin scheme in primitive variables, where the pressure terms, deliberately omitted in Eq. (3), cancel out in the weak projection and the spectral approximation identically satisfies (4). The resulting dynamical system of amplitudes is numerically integrated in time by means of a fourth order linearly implicit backward differences scheme combined with standard fourth order Adams-Bashforth extrapolation of the nonlinear term. The spatio-temporal convergence and reliability of the numerical method have been extensively tested in previous works.[6,12,26,27] For a vast exploration, the spatial resolution used in the domain $\mathfrak{D}$ is $M_r \times N_\theta \times L_z = 25 \times 33 \times 33$ radial $\times$ azimuthal $\times$ axial grid points, and $M_r \times N_\theta \times L_z = 33 \times 33 \times 33$ for further refinements, resulting in a dynamical system of nearly 3.5×10^4 degrees of freedom. No substantial differences have been observed when increasing the spatial resolution or decreasing the time step. The spatial convergence has been checked by repeating some test computations on a finer mesh of $M_r \times N_\theta \times L_z = 41 \times 49 \times 49$. Also the energy contents of the highest axial/azimuthal Fourier modes has been monitored for every single run to ensure the adequacy of the spatial truncation. For subcritical runs, an energy decay of 6 to 7 orders of magnitude below that of the basic flow has been considered enough. Transitional runs are clearly underresolved when turbulent motion begins. The computational costs of the resolution that would be required are unaffordable, but one must bear in mind that it is not the aim of this study to simulate turbulence, but to bound the basin of attraction of the basic flow. Computations for a longer pipe have been carried out in order to check the length effects in the transition mechanisms studied. In particular, computations with $\Lambda = 32\pi \sim 100$ have been done by increasing the grid size to $M_r \times N_\theta \times L_z = 33 \times 33 \times 129$.

The *normalized energy* of a perturbation $\mathbf{u}$ is measured by means of the volume integral or Hermitian product

$$\varepsilon(\mathbf{u}) = \frac{1}{2E_{\mathrm{HP}}}\int_{\mathfrak{D}} \mathbf{u}^\dagger \cdot \mathbf{u} d\mathfrak{D}, \tag{5}$$

with respect to the energy of the basic Hagen-Poiseuille flow, $E_{\mathrm{HP}} = \pi\Lambda/6$, so that the *amplitude* of the perturbation is defined as the square root of its normalized energy,

$$A(\mathbf{u}) = \sqrt{\varepsilon(\mathbf{u})}. \tag{6}$$

To better understand how the energy is distributed within the flow, it is very convenient to express the perturbed velocity $\mathbf{v}$ as a sum of the basic flow $\mathbf{u}_b$ and the Fourier components of the perturbation field $\mathbf{u}$, satisfying (3), (4), and (2),

$$\mathbf{v}(r,\theta,z,t) = \mathbf{u}_b(r) + \mathbf{u}_{00}(r,t) + \overbrace{\sum_{n\neq 0} e^{in\theta}\mathbf{u}_{0n}(r,t)}^{\mathbf{u}_{2\mathrm{D}}(r,\theta,t)} + \overbrace{\sum_{l\neq 0}\sum_{n} e^{i(n\theta+2\pi/\Lambda lz)}\mathbf{u}_{ln}(r,t)}^{\mathbf{u}_{3\mathrm{D}}(r,\theta,z,t)}, \tag{7}$$

where $\mathbf{u}_{00}$ contains the azimuthal-axial-averaged perturbation velocity profile, $\mathbf{u}_{2\mathrm{D}}$ represents the nonaxisymmetric streamwise component of the velocity field and $\mathbf{u}_{3\mathrm{D}}$ the remaining streamwise-dependent components. For the particular computations presented throughout this study, $\mathbf{u}_{2\mathrm{D}}$ must be interpreted as the streaks modulation of the flow.

Using (5) on the decomposed velocity field, the energies corresponding to the bulk flow, to the streamwise component and to the 3D perturbation can be computed independently as $\varepsilon_{00} = \varepsilon(\mathbf{u}_{00})$, $\varepsilon^{2\mathrm{D}} = \varepsilon(\mathbf{u}_{2\mathrm{D}})$ and $\varepsilon^{3\mathrm{D}} = \varepsilon(\mathbf{u}_{3\mathrm{D}})$, respectively.

Subcritical instability in shear flows is efficiently triggered by adding streamwise vortical perturbations to the basic flow.[11,14–16] Of all possible initial disturbances, streamwise vortices with azimuthal wave number $n_v = 1$ are the best candidates to trigger transition, as several linear nonmodal stability analyses of pipe flow[6,13] have repeatedly shown that this sort of disturbances exhibit optimal transient growth. This energy growth leads to the generation of strong nonlinear streaks, in the presence of which streamwise-dependent modes of selected axial periodicity are destabilized. Time-dependent linear stability analysis of the streamwise streaks[28] confirms that only a subset of streamwise-dependent modes are potentially destabilized by the inflectional transitional streaks. Therefore, the perturbation introduced at $t=0$ must satisfy three requirements to be *optimal*. First, it must have a strong streamwise component to generate inflectional profiles or streaks. Second, it must also contain small streamwise-dependent components of suitable axial periodicity within the range that exhibits optimal inflectional instability.[28] Third, since the streaks are transient modulations of the basic flow, the destabilized streamwise-dependent components have a limited period of time to grow and nonlinearly interact with the modulated flow while it lasts. As a result, although the streamwise-dependent initial amplitudes can be of much smaller magnitude than that of the streamwise component, they still need to be large enough to be able to break the streaks before the onset of their viscous decay.

Even though a single pair of streamwise vortices ($n_v = 1$, from here on referred to as N_1) experiences the largest transient growth,[6,13] perturbations consisting of a greater number of pairs of streamwise vortices ($n_v = 2, 3, \ldots$, which we will call N_2, N_3, …, respectively), although exhibiting smaller transient growth, might develop into streaks with a higher potential of destabilizing streamwise-dependent waves.

The initial disturbance $\mathbf{u}_0 = \mathbf{u}(r,\theta,z,0)$ used in a first exploration of the critical threshold consists of a suitable superposition of a single pair of two-dimensional streamwise vortices (N_1), $\mathbf{u}_0^{2\mathrm{D}}$, and a set of three-dimensional waves, $\mathbf{u}_0^{3\mathrm{D}}$, of selected axial periodicities,

$$\mathbf{u}_0 = \overbrace{C^{2D} e^{i\theta} \mathbf{v}_1(r)}^{\mathbf{u}_0^{2D}} + \overbrace{\sum_{l,n} C_{ln}^{3D} e^{i(n\theta + k_o l z)} \mathbf{v}_n(r)}^{\mathbf{u}_0^{3D}} + \text{c.c.}, \tag{8}$$

where c.c. stands for complex conjugated terms. The radial structure of $\mathbf{u}_0^{2D}$ takes the simplest polynomial form compatible with solenoidality and nonslip boundary conditions at the wall, closely resembling a nearly optimal (in its capability of generating strong streaks) pair of streamwise vortices.[13,28] As for $\mathbf{u}_0^{3D}$ in (8), the sum only excites streamwise dependent modes with $n=\{-1,0,1\}$ and $l=\{l_1,l_2,l_3\}$ (i.e., 9 streamwise modes overall) and whose radial structure is also of the lowest polynomial order. The radial fields just described are:

$$\mathbf{v}_j(r) = \begin{cases} r(1-r^2)\hat{\boldsymbol{\theta}} & j=0 \\ -ijr^{\sigma-1}(1-r^2)^2\hat{\mathbf{r}} + D[r^\sigma(1-r^2)^2]\hat{\boldsymbol{\theta}} & j\neq 0, \end{cases} \tag{9}$$

where $\sigma=1$ (2) for j odd (even) and D denotes a radial derivative. The subscript j alternatively equals 1 for the 2D component or represents n for the 3D component of the perturbation given in (8).

The fundamental axial wave number $k_o=2\pi/\Lambda$ appearing in (8) is determined by the aspect ratio of the computational pipe domain. The triad $i=1,\ 2,\ 3$, must then be chosen so that the excited axial wave numbers ($k_i=k_o l_i$) lie within the range exhibiting optimal exponential growth of $\mathbf{u}^{3D}$ in the presence of the streaks developing from $\mathbf{u}_0^{2D}$. According to former studies[12,28] and a few preliminary runs within the frame of the present work, the optimal axial wave number appears to be somewhere in the interval $k_{opt} \in [1.5, 2.2]$. Since the aspect ratio of the pipe has been fixed to $\Lambda \sim 20$ radii, the triad $l_i=\{6,7,8\}$, which activates waves with $k_i=\{1.56, 1.88, 2.19\}$, must be initially excited.

The complex constants C^{2D} and C_{ln}^{3D} in (8), which modulate the initial amplitude of the two components of the perturbation, are chosen so that the initial energy of the streamwise vortices, $\varepsilon(\mathbf{u}_0^{2D})$, and of the three-dimensional waves, $\varepsilon(\mathbf{u}_0^{3D})$, take the desired values ε_0^{2D} and ε_0^{3D}, respectively. ε_0^{3D} is evenly distributed among the whole set of excited 3D modes. The complex phases of these constants are generated randomly.

With the aim of testing vortical perturbations of different azimuthal topology, a slightly different type of initial condition has been defined. The 2D component in (8) has been adapted in (10) to admit varying azimuthal wave numbers (n_v) in order to represent streamwise-independent structures consisting of an arbitrary number of pairs of vortices. The simplest polynomial form, detailed in (9), has been retained, with j now representing n_v. Thus, vortical structures with $n_v=2,3$ (N_2, N_3) can be considered along with the aforementioned single pair of vortices ($n_v=1$, N_1). No studies exist, to the authors knowledge, on the optimal range of axial wave numbers (k) of the waves that are most destabilized in the presence of streaks developing from N_2 and N_3 vortical structures. Consequently, rather than undertaking such a vast task as would be determining the optimal axial wave numbers, a decision has been made of simply adding a random 3D noise, which in fact narrowly mirrors what happens in experiments, thus exciting 3D waves of all axial wavelengths. The exploration for a single pair of vortices (N_1) has been repeated with this random 3D noise for checking purposes. The general expression of the initial disturbance for this enhanced parameter exploration is

$$\mathbf{u}_0 = \overbrace{C^{2D} e^{i n_v \theta} \mathbf{v}_{n_v}(r)}^{\mathbf{u}_0^{2D}} + \overbrace{\mathbf{u}_{\text{rand}}(r,\theta,z)}^{\mathbf{u}_0^{3D}} + \text{c.c.}, \tag{10}$$

with $\mathbf{u}_{\text{rand}}$ a random perturbation velocity field of the desired amplitude, containing much lower energy than the streamwise component.

III. CRITERIA FOR TRANSITION

In order to establish criteria to decide whether the perturbations (8) and (10) lead to turbulence or not, it is crucial to run up to a *time-horizon* at which the streaks have fully developed and the three-dimensional perturbations have had enough time to grow. This time has been found to be at least $T_{max}=1000$ advective time units for the lowest ε^{2D} at the highest Re explored. After this period, either the streak breakdown or the irreversible onset of viscous decay have taken place. However, for $\text{Re}<7500$, $T_{min}=600$ has been found to be enough. Experimentally, considering the perturbation is at worst advected downstream at the basic flow maximum axial speed, this is equivalent to having the observation point at 300–500 diameters distance downstream from the perturbation point. The longest constant mass flow rig used in experiments allows us to make observations up to 530 diameters downstream from the perturbation location,[9] which our time horizons represent well enough. Checking for turbulence after this time is therefore a reasonable approach, and this is done by a bare eye inspection of the modal energy distribution. In the present study, a simulation run is considered *turbulent* if

$$\varepsilon^{3D}(T) \geqslant 10^{-3} \text{ and } \mathcal{O}(\varepsilon^{2D}(T)) \sim \mathcal{O}(\varepsilon^{3D}(T)), \tag{11}$$

otherwise *laminar*. Condition (11) is based on the fact that three-dimensionality is a clear signature of turbulent dynamics and therefore it is required for the streamwise-dependent modes to be still active, and much stronger than initially, at the end of the run. For low Re, however, transition for a limited time window with an eventual relaminarization has been consistently observed. These *relaminarized* runs would have appeared as turbulent depending on the position of the observation area in an experimental rig. The existence of this phenomenon suggests that some of the runs considered within a time horizon of $T=600$ may have relaminarized if longer runs had been envisaged. It is however important to point out that we do not expect to properly model developed turbulence with our discretization, as it is too coarse to represent the smallest turbulent scales at which the energy is dissipated. Turbulence and relaminarization are therefore a misrepresented phenomena in the current work, and should be interpreted with extreme care. Figures 1(a)–1(c) illustrate

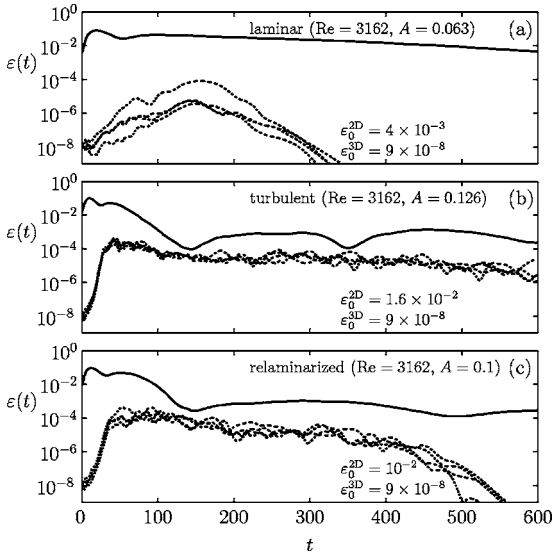

FIG. 1. From top to bottom, (a) laminar, (b) turbulent, and (c) relaminarized runs. In all three plots, the continuous line represents $\varepsilon^{2D}(t)$, and the dotted lines are the energies associated with the streamwise-dependent triads.

a laminar, a turbulent and a relaminarized run, respectively. They all depict the evolution of N_1-type disturbances and the selected set of optimal 3D waves. In each plot, the continuous line corresponds to the energy of the mode excited by the streamwise perturbation, which constitutes a reliable signature of the development of the streaks. The dashed lines are the energies associated with some of the streamwise-dependent modes of the axial triads with $n=0$ or $|n|=1$. In the laminar case, Fig. 1(a), the three-dimensional components of the perturbation are only temporarily excited once the streaks have developed, but this tendency is soon reverted and their energy rapidly decays before having been able to perturb the streamwise streaks. The turbulent run, Fig. 1(b), differs from the laminar one in the growth rate of the streamwise dependent modes in the presence of the streaks, eventually leading to a streak breakdown and setting off chaotic dynamics or turbulent motion. This phenomenon can be spotted by looking at the drastic fall of $\varepsilon^{2D}(t)$ for $t>50$. Since the inflectional structure of the modulated flow is streamwise independent, this transition scenario leads to *global* turbulence instead of the *intermittency* phenomena observed in the experiments, where coexistence of laminar flow with turbulent regions, usually called *puffs* and *slugs*, is observed. Finally, in the relaminarized run, Fig. 1(c), the turbulent motion is abruptly interrupted and the streamwise-dependent energies start decaying rapidly whilst the streaks recover temporarily to slowly vanish afterwards for $t>600$.

IV. RESULTS AND DISCUSSION

For the present study, we have carried out a comprehensive exploration of the minimum initial amplitude, $A_0=A(\mathbf{u}_0)$, defined in (6) required to trigger transition, according to the criteria established in Sec. III. This has initially been done for disturbances fulfilling all optimality criteria derived from previous studies, i.e., a single pair of streamwise vortices, N_1, plus the 3D waves that are most unstable to the streaks developed from these vortices, detailed in (8).

The current exploration has been extended for disturbances consisting of different numbers of pairs of vortices (N_2 and N_3), on top of which random 3D noise has been added according to (10), since no available data on the optimal axial periodicity of 3D waves destabilized by streaks developing from these vortices is available in the literature. The critical threshold exploration for N_1 disturbances has been repeated with random 3D noise to allow comparison with the previous exploration only considering activation of the optimal 3D waves, and to indeed assess their optimality. Finally, the critical amplitude threshold for the N_1 type of initial condition exciting the optimal 3D waves has been recomputed on a much longer pipe in order to rule out length scale effects on transition for the particular scenario investigated. An extra run on the long pipe with random 3D noise added on top of an N_1 vortical disturbance has been computed to illustrate the streak breakdown global mechanism of transition by comparing the same case on the short pipe.

A. N_1 disturbances with optimal 3D waves

The critical amplitude threshold exploration for this particular kind of disturbances covers a wide range of Reynolds numbers, within the interval $\mathrm{Re}\in[2.5\times10^3, 1.26\times10^4]$, and initial energies ε_0^{2D} within the range $\varepsilon_0^{2D}\in[2.5\times10^{-5}, 4\times10^{-2}]$, while the energy associated with the streamwise-dependent modes is held constant, with $\varepsilon_0^{3D}=9\times10^{-8}$ evenly distributed among the corresponding triads.

Results for the coarse computations ($M_r\times N_\theta\times L_z=24\times33\times33$), are shown in Fig. 2(a), where white triangles represent laminar runs, black circles denote turbulent runs, and empty circles correspond to relaminarized runs. The *critical* amplitudes, obtained from a refined exploration ($M_r\times N_\theta\times L_z=33\times33\times33$), have been marked with gray squares. Overall, the over two hundred exploratory runs required nearly 10 CPU months on a 3 GHz Athlon-PC cluster.

For low Reynolds numbers, it is remarkable how relaminarization is a very common phenomenon, where the basic flow preserves sound stability properties and considerably big perturbations are required to trigger transition. As expected, the critical amplitude A_c is a decreasing function of the Reynolds number. In fact, A_c exhibits a vertical threshold evidenced by the behavior of the slope, which is very pronounced at low Re (allegedly converging to a vertical asymptote at $\mathrm{Re}_{cr}\lesssim2000$).

As soon as Re is increased, the numerical results shown in Fig. 2(a) clearly suggest that pipe Poiseuille flow follows the same behavior as other shear flows,[15,16] with a critical amplitude that decreases with Re according to $A_c\sim\mathrm{Re}^{-1.47\pm0.02}$, very close to the exponent $\gamma=-3/2$ quoted in previous numerical studies with far less resolution and run on a much shorter domain[12] (dashed straight line in Fig. 2), at least within the studied range. This behavior has been confirmed by increasing the spectral resolution of the numerical scheme. Furthermore, the axial/azimuthal resolutions have been validated as sufficient by assessing the decay of

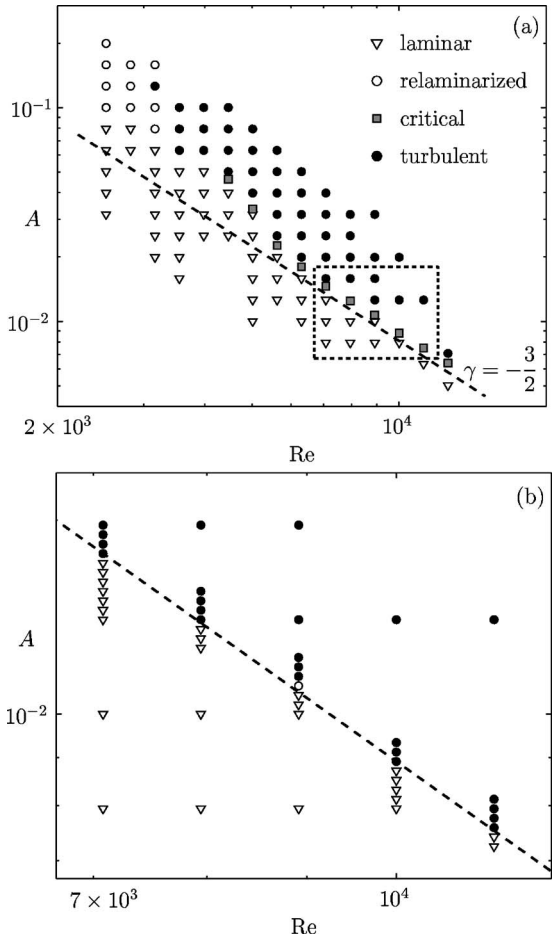

FIG. 2. Threshold amplitude for N_1-type perturbations with optimal 3D waves. (a) Coarse exploration with lower spectral resolution $M_r \times N_\theta \times L_z = 24 \times 33 \times 33$. (b) Zoomed region on top, showing the numerical refinements for $M_r \times N_\theta \times L_z = 33 \times 33 \times 33$. Overall, the 200 runs presented here required nearly 10 CPU months on a 3.0 GHz Athlon PC cluster.

the energy contents of the highest Fourier modes for the subcritical runs, which has been required to be 6 to 7 orders of magnitude below that of the basic flow. The resolution is certainly not sufficient for runs exhibiting transition once turbulence sets in. However, since this work is only concerned with bounding the basin of attraction of the basic flow, properly representing the laminar phases of the transition process is enough. The uncertainty on the exponent γ has been assessed by estimating the evolution of the slope of the critical threshold through linear regressions on subsets of contiguous data points and by assessing the variability of this slope around the average value at which it seems to stabilize at high Reynolds. Figure 2(b) shows a zoom on the squared out region in Fig. 2(a), including the higher resolved integrations that have been used to accurately determine the threshold amplitude.

The experimental results recently reported in HJM revealed a clear exponent $\gamma = -1$. The numerical simulations presented here are not necessarily in contradiction with the experiments. In fact, expression (1) implicitly involves many physical aspects that require an accurate description before making any comparison between numerics and experiments. First, the mathematical definition of the amplitude A appearing in (6) was provided in terms of the kinetic energy of the perturbation, whereas HJM measured the amplitude A as a ratio between the perturbing injected flux and the basic mean flux, i.e., $A \sim \Phi_{\text{inj}}/\Phi_{\text{HPF}}$. Second, the geometrical features of the perturbation will necessarily condition the subspace over which we are measuring the amplitude appearing in (1). In the present scenario, we have selected streamwise-independent disturbances that optimally trigger inflectional instability, whereas in the experiments, the disturbances are axially localized, thus exciting the full spectrum of streamwise wave numbers. Besides, the azimuthal symmetry of the numerical perturbation is $n_v = 1$, in contrast to the six-jet device used in HJM that forces an $n_v = 6$ symmetry. Third, our perturbation mechanism is mathematically posed as an *initial value problem*, whereas the injections used in HJM require finite durations, thus transiently modifying the original topological features of the basin of attraction. Finally, expression (1) is only valid for high values of Re. Thus, over the range studied both in experiments and numerics the exponent obtained must necessarily be *local*. This would also be in line with results obtained for plane Poiseuille flow,[16] where full simulations at low Re also give different exponents that are ascribed to *finite*-Re effects. Further increase of the Reynolds number would be required to asymptotically confirm the value of γ.

The observed discrepancies with experiments should not be taken as a major hindrance. We are concerned with natural transition due to unknown perturbation sources that are always present in the flow. The aim of this study is to identify the components of this unknown sources that can be held responsible for transition and, to that end, numerical simulation is much more flexible than experiments. We are quite confident, however, that experimental disturbances containing strong components of the numerically used ones are realizable and that they will very much yield the same results as our numerical experiments.

B. $N_{1,2,3}$ disturbances with random 3D noise

To gain some understanding on the effect on transition of the azimuthal topology of the initial disturbance, a systematic search for the critical amplitude threshold has been implemented based on initial conditions consisting of $n_v = 1$, 2, and 3 pairs of rolls (N_1, N_2, and N_3 disturbances). As previously stated, the objective is to test their presumed higher capability of destabilizing 3D waves despite their lesser transient growth when compared with N_1 perturbations. Ideally, we would have liked to test azimuthal wave numbers of up to $n_v = 6$ so as to allow direct comparison with the 6-jet experimental injection used in HJM, but the azimuthal resolution this would require renders such an exploration unaffordable.

Lacking insight on the most rapidly growing axial wave numbers, the 3D component of the perturbation has been introduced as a random velocity field fairly evenly distributing among all modes an energy four to five orders of magnitude below that of the streamwise vortices. The objective is to make sure the optimal 3D waves are activated, notwith-

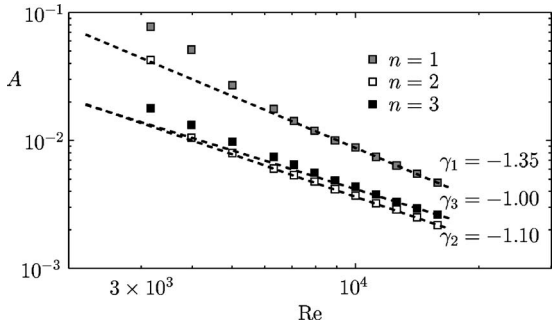

FIG. 3. Critical amplitude threshold as a function of Re for initial disturbances made up of $n_v=1,2,3$ pairs of vortices and a much lower random 3D noise.

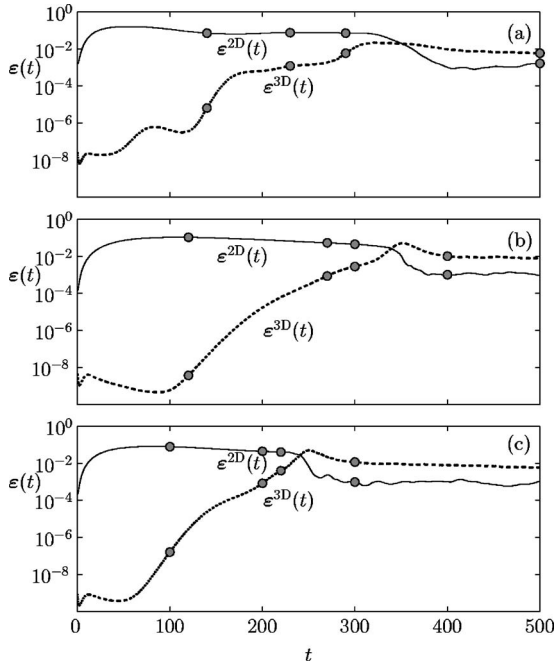

FIG. 4. From top to bottom, energy-evolution plots of streak breakdown transition examples for vortical perturbations of the (a) N_1, (b) N_2, and (c) N_3 types, for Re=5012. In all three cases, the added 3D component is a random field.

standing the fact that some spurious energy is being wasted on irrelevant modes. No significant differences on the critical threshold should *a priori* be expected from using a random 3D perturbation instead of 3D waves within the optimal axial wave-number range. While the approach of adding a random perturbation is of much simpler implementation, the possibility of identifying the optimal waves by comparison with computations exciting exclusively certain (optimal) wave numbers, can be very valuable, since it may be relevant to understanding transition and can help establish connections with recently found travelling-wave solutions,[20,21] some of which have wavelengths in the vicinity of the optimally destabilized 3D perturbations.

Thus, the critical threshold for N_2 and N_3 has been obtained and the one for N_1 is recomputed for disturbances with a random 3D component, using the initial condition presented in (10). Over 100 additional runs with a spatial resolution of $(M_r\times N_\theta\times L_z=33\times33\times33)$ have been performed to bound the critical threshold for the three different types of initial disturbance. Figure 3 shows the critical amplitude thresholds of N_1, N_2, and N_3 disturbances with random 3D noise added. The estimated asymptotic exponents, resulting from the analysis through linear regression of the evolution of the slope, are displayed with dashed straight lines.

A first obliged remark is that, for N_1, adding a random noise instead of activating the right axial wavelengths, as was done in the first exploration, does not alter the picture substantially. This seems to confirm that a small packet of waves can be held responsible for transition, the rest of modes playing no role whatsoever until the streaks have been broken and chaotic motion has set in. The exponent, however, seems to have slightly decreased to a value of $\gamma_1\sim-1.35\pm0.02$, which is less pronounced than the previously found $\gamma=-1.47\pm0.02$. Exciting nonoptimal wavelengths seem to deteriorate the capability of the 3D disturbance to bring about transition as Re is increased, as though competing waves were disturbing one another through nonlinear interaction, thus deferring transition.

The critical thresholds for N_2 and N_3 appear to be of a similar order of magnitude and both considerably lower than that for N_1, for moderate values of Re. It is therefore clear that, within the studied Re range, initial disturbances consisting of a couple of pairs of streamwise vortices are slightly more effective than those consisting of three pairs and considerably better than a single pair of vortices. However, it is not immediately clear whether this will still be the case at higher Re. Assuming the asymptotic regime of the critical threshold has more or less been established by the time we reach the right end of the explored Re range, N_1 disturbances stand a better chance of dominating the transition threshold for Re tending to infinity, as N_2 disturbances produce an exponent $\gamma_2\sim-1.10\pm0.03$ and N_3 disturbances a $\gamma_3\sim-1.06$, not yet stabilized but apparently tending towards -1. Nevertheless, the possibility that all disturbance thresholds mellow out asymptotically to an exponent $\gamma\sim-1$ cannot be discarded nor proved from the present study, since the exponent stabilization may be apparent and its evolution could resume at higher Re.

To the difficulty of discussing the current results, we must add a further hindrance, namely, that the critical amplitude at a given Re depends on the initial energy of the 3D component of the perturbation, which is assumed to be very small compared to the 2D component to ensure the streak breakdown mechanism, and not oblique transition, takes place. Chances are that the 3D perturbation energy level has an effect on the critical threshold at moderate Re but a rather weak one on its asymptotic exponent, since as Re increases the streaks lifetime stretches giving a longer time for the 3D waves to grow, thus making their initial energy level irrelevant as long as it is finite. Figures 4(a)–4(c) exemplify the streak breakdown mechanism for the N_1, N_2, and N_3 types of initial disturbance, respectively. Depicted are the time evolution of the energy of the streaks (ε^{2D}, solid line), together with that of the 3D component (ε^{3D}, dashed line). All three runs correspond to Re=5012 and initial perturbations which are just supercritical ($A_1=2.75\times10^{-2}$, $A_2=8.13\times10^{-3}$, and

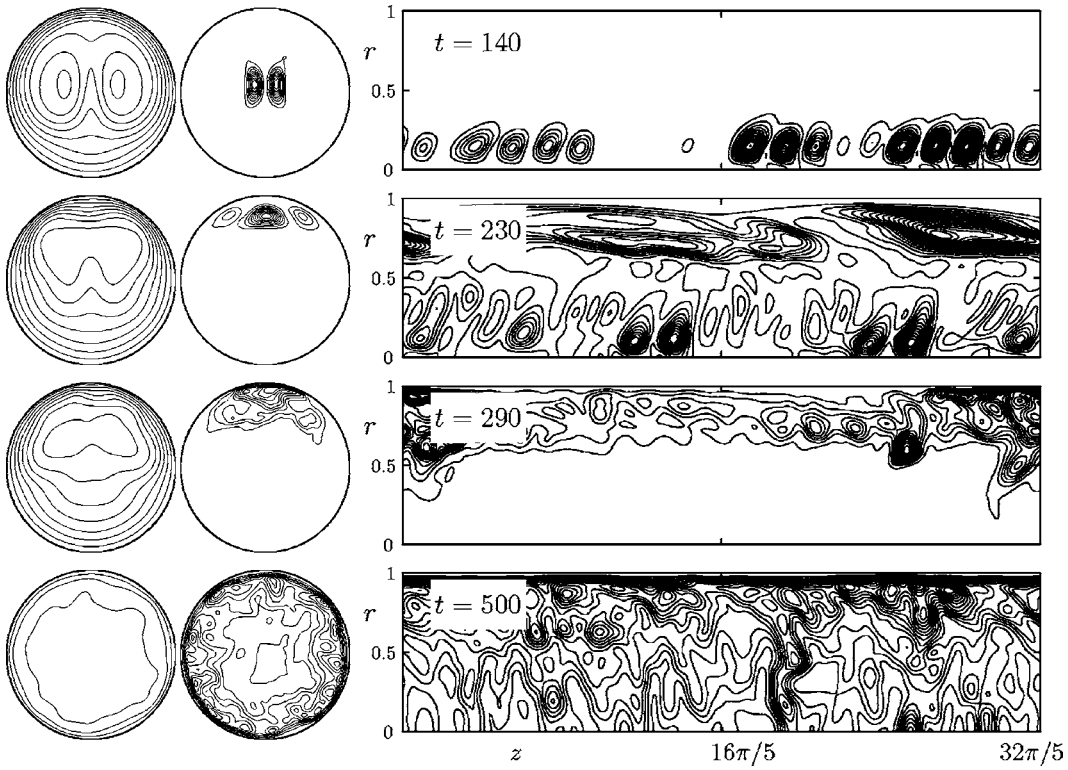

FIG. 5. From left to right, contours of $\langle w\rangle_z$, $\langle \varepsilon^{3D}\rangle_z$ and $\langle \varepsilon^{3D}\rangle_\theta$, for the N_1 disturbance evolution with $\Lambda=20.1$ and $\mathrm{Re}=5012$. Time elapses from top to bottom, with snapshots taken at the most relevant instants, marked with gray circles in Fig. 4(a).

$A_3=10^{-2}$, for the N_1, N_2, and N_3 cases, respectively). As expected, in all three cases the streaks develop and excite 3D modes that start growing exponentially until they acquire sufficient energy to nonlinearly interact with the streaks and bring about transition. The N_1 case exhibits a slightly more complex behavior as the different stages of the 3D perturbation energy growth evince.

In Figs. 5–7, three series of snapshots at selected times, conveniently indicated with gray circles on the energy evolution plots [Figs. 4(a)–4(c)], help illustrate the streak breakdown process for each type of vortical disturbance. On the left of Figs. 5–7 z-averaged cross-sectional contours of the axial speed component of the flow $\mathbf{v}=(u,v,w)$ are represented within the range $0\leqslant\langle w\rangle_z(r,\theta,t)\leqslant 1$ in order to visualize the streaks formation and destabilization. The center and right vertical sequences of pictures correspond to energy density contours of the velocity component $\mathbf{u}_{3D}(r,\theta,z,t)$ appearing in (7). More specifically, the central array of figures contains z-averaged cross-sectional contours, while the right array shows θ-averaged contours on a transversal section $(r,z)\in[0,1]\times[0,\Lambda]$. The aforementioned energy density averages are given by

$$\langle \varepsilon^{3D}\rangle_z(r,\theta,t)=\frac{1}{2}\int_0^{\Lambda}\|\mathbf{u}_{3D}(r,\theta,z,t)\|^2 dz, \tag{12}$$

and

$$\langle \varepsilon^{3D}\rangle_\theta(r,z,t)=\frac{1}{2}\int_0^{2\pi}\|\mathbf{u}_{3D}(r,\theta,z,t)\|^2 d\theta, \tag{13}$$

and their contours are drawn in arbitrary units. In addition, the axial coordinate of the longitudinal sections has been conveniently scaled to aid representation. These series of contours reveal the modal structure of the 3D waves as well as their location and destabilization effects over the streaks. A fixed number of contour lines is extrapolated between 0 and the maximum energy at each particular instant of time.

Because of their simplicity, it seems natural to start by discussing the N_2 and N_3 cases, shown in Figs. 6 and 7, respectively. The 3D perturbation organizes itself and grows exponentially in the vicinity of the saddle lines of the streaks-modulated axial velocity profiles, as can be seen in the snapshots at $t=120$ for N_2 and $t=100$ for N_3. Once the 3D perturbation has reached a sufficient energy level, nonlinear interaction with the streaks starts ($270\leqslant t\leqslant 300$ for N_2 and $200\leqslant t\leqslant 220$ for N_3), destabilizing the laminar profile and leading to turbulence. It should be noted that the axial structure of the 3D waves is neither long nor stretching, which could be taken as evidence that the transition scenario investigated does not contemplate the possibility of local transition or intermittency phenomena, plausibly rendering results fairly independent of the pipe length considered. It should also be noted that the structures shown in the longitudinal sections of Figs. 5–7 are being advected downstream

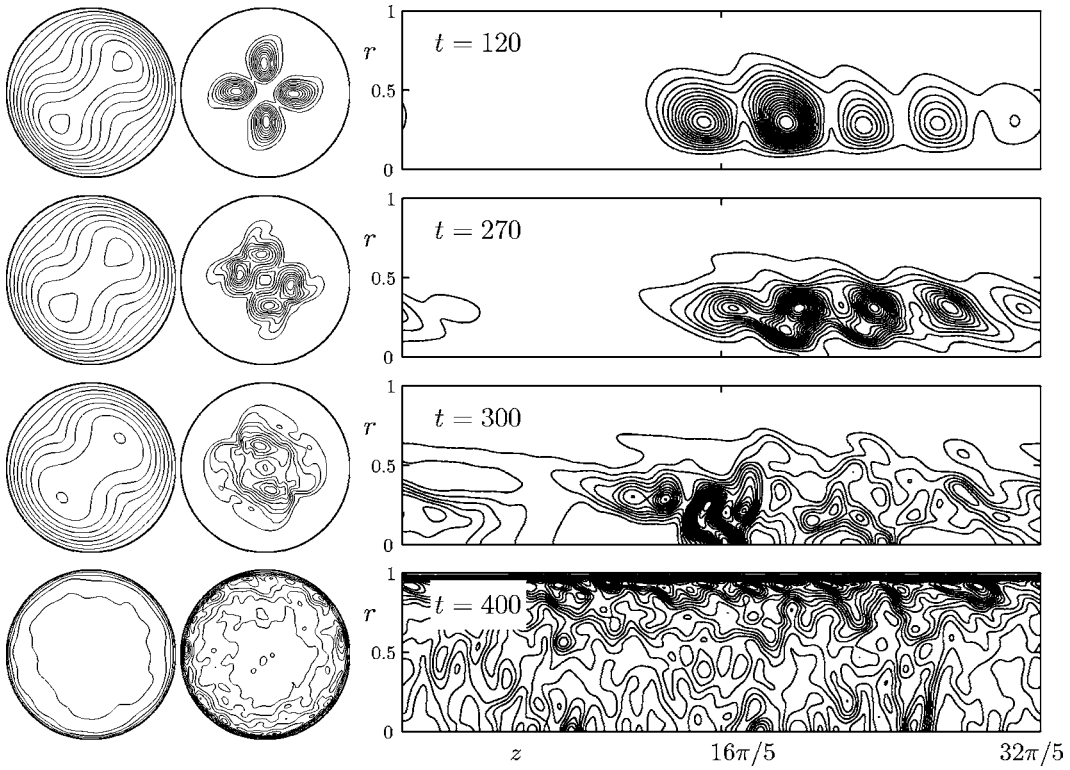

FIG. 6. Same as Fig. 5, for the N_2 perturbation. Snapshots are taken at instants marked with gray circles in Fig. 4(b).

and hence re-enter the domain from the left as soon as they leave it through the right-end due to the axial periodicity.

Conversely to what happens in the N_2 and N_3 cases, the N_1 case admits no easy interpretation, as several 3D modes seem to compete at different stages of the streaks formation and development. In a first stage, the 3D perturbation seems to be transiently concentrated near the wall, where the axial velocity gradients are largest (not shown in Fig. 5), to be

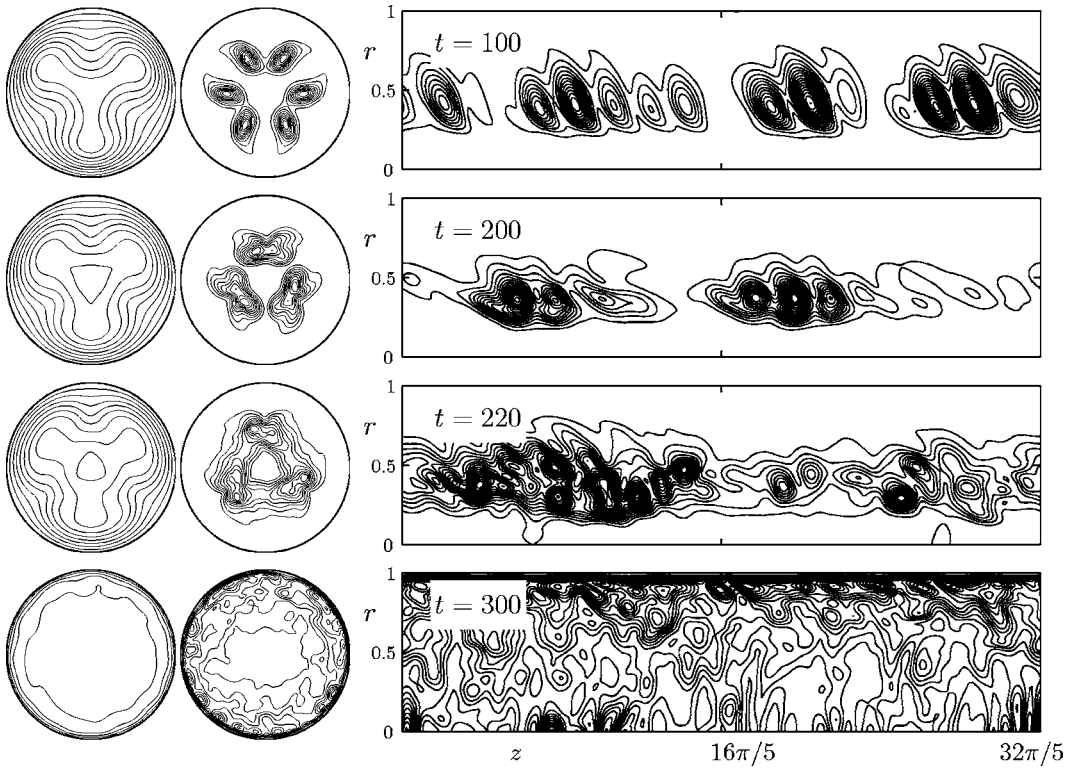

FIG. 7. Same as Fig. 5, for the N_3 perturbation. Snapshots are taken at instants marked with gray circles in Fig. 4(c).

eventually absorbed by a stronger perturbation that grows up closer to the pipe centerline, in the vicinity of the saddle lines of the axial velocity profile ($t=140$ in Fig. 5). This centered perturbation grows rapidly until it saturates and is then overtaken again by near-wall components ($t=230$) that eventually destabilize the streaks ($t=290$) and trigger transition. The wavelength of the dominant perturbation at each stage of the process varies. Long wavelengths only become dominant in the last stages before transition.

C. Pipe length effects on transition

The streak breakdown mechanism is based on the development of a global inflectional profile affecting the whole pipe length. The mathematical explanation is provided when studying the streamwise invariance of the $\mathbf{u}^{2D}$ introduced initially. The structure of Eq. (3) preserves streamwise independence of $\mathbf{u}^{2D}(t)$ due to the fact that the disturbance has spanwise components only, whereas the basic flow is purely streamwise. Therefore, upon streaks generation, saddle points, or rather saddle streamwise lines, appear along the pipe, resulting in an inflectional instability of the $\mathbf{u}^{3D}(t)$ components destabilizing the whole pipe length at once. The inflectional stability thus generated has been numerically shown to follow selection rules as to which axial wave numbers can be destabilized by the streaks.[12,28] The streak breakdown transition process happens to be clearly dominated by medium-short wavelengths of order $\mathcal{O}(\lambda)\sim\pi$. Hence, no substantial discrepancies can be expected when repeating the computations on a longer aspect-ratio pipe.

Intermittency is a commonly observed phenomenon in experimental pipe transition. Perturbations initially localized in space lead to small patches of turbulent motion called *slugs* that, while convected downstream, grow into the surrounding laminar regions to end up filling the whole pipe domain. To properly capture this behavior numerically, long enough computational domains need to be set up for these long-scale turbulent structures to show up and grow freely. The aspect ratio we have used so far ($\Lambda=6.4\pi\sim20$) is clearly too short to allow for intermittency phenomena, whose characteristic length has been shown to be bigger.[25,29] However, the transition mechanism studied here is *global*; hence, not depending on the formation of long structures, but of medium-short ones.

To assess the pipe-length effects on streak-breakdown transition, we have computed the critical threshold for N_1 disturbances, exciting only the optimal 3D waves, but this time on a much longer pipe of $\Lambda=32\pi\sim100$. To preserve a somewhat sufficient representation of the small axial scales, the axial grid points count has been four-folded to produce a mesh of $M_r\times N_\theta\times L_z=33\times33\times129$. The triads $l_i=\{30,35,40\}$ for $|n|=0,1$ in (8) have been excited to activate the same 3D waves that were activated in the short pipe version, i.e., $k_i=\{1.56,1.88,2.19\}$. Table I reports the critical amplitudes for the long and the short pipe. It is reasonably clear from the compared results that no significant differences are introduced by a pipe elongation, at least for computational domains of up to 100 radii.

As a last verification that pipe-length effects are of little importance in the streak breakdown transition scenario, the evolution of N_1-type disturbances defined in (10) and shown in Figs. 4(a) and 5 have been computed on the longer computational domain. An exact evolution cannot be expected in any case, since the random 3D energy, now distributed among extra axial modes that were not present in the short pipe case, makes a perfect timing unachievable. Also the slight reduction of axial resolution, inevitable to compute on such a long domain, may have an effect on the results.

TABLE I. Critical amplitude threshold as a function of Re for initial disturbances made up of a single pair of vortices and waves of selected axial periodicity derived from computations on a short ($\Lambda\sim20$ radii) and a long ($\Lambda\sim100$ radii) pipe.

	A_{cr}	
Re	Short pipe	Long pipe
4467	4.6×10^{-2}	4.7×10^{-2}
5012	3.3×10^{-2}	3.3×10^{-2}
6310	1.8×10^{-2}	1.8×10^{-2}
8913	1.1×10^{-2}	1.1×10^{-2}
12589	6.4×10^{-3}	6.4×10^{-3}

Figure 8 shows the energy-evolution plot for the N_1 disturbance on the long pipe, to be compared to that on the short pipe [Fig. 4(a)]. The streaks development is completely analogous. As for the 3D component of the perturbation, the agreement is reasonably good but for a couple of discrepancies that need comment. First, at the very initial stages of the streaks formation, the short pipe exhibits 3D energy oscillations that are not present in the long pipe. The reason is that the long pipe simulation takes into account modes with very low axial wave number, not captured in the short pipe version. These modes are known to experience large algebraic transient growth that could be masking the organization of the 3D waves that are to be destabilized later by the streaks. Second, in the latter stages before transition, the short pipe seems to hesitate a bit longer before bringing about streak breakdown. The slightly diminished axial resolution of the longer pipe, thus dissipating less energy in the small scales could be at the origin of the slightly faster transition. Another possible explanation for the faster transition on the long pipe when compared with the short one could be derived from the random properties of the 3D noise. If, as we hypothesize, the streak breakdown transition is global and only depends on short-medium wavelengths, the long pipe could be behaving as a mere concatenation of short pipes, each with its particu-

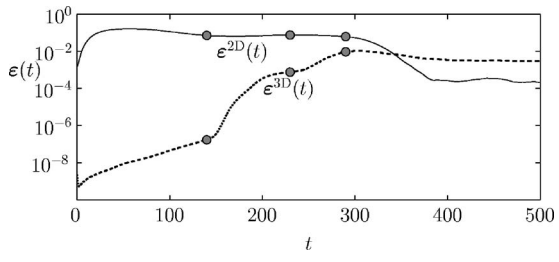

FIG. 8. Same as Fig. 4(a), but computed on the long pipe.

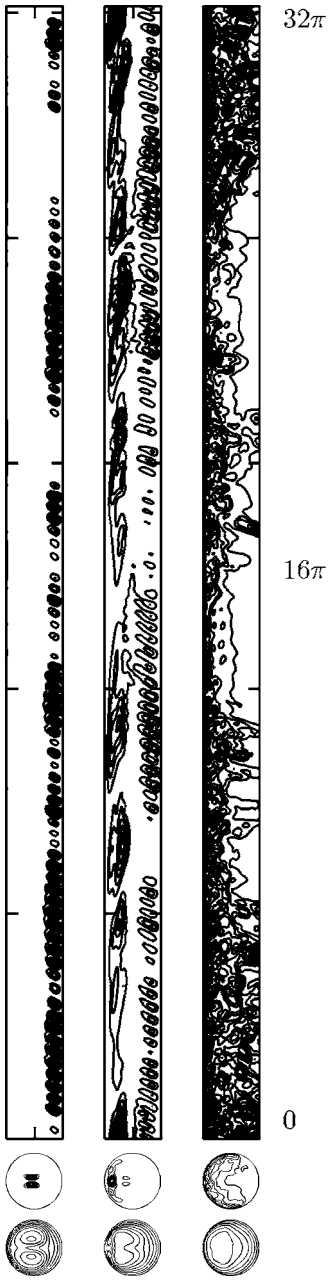

FIG. 9. Same as Fig. 5, but on the long pipe with $\Lambda=100.5$. Snapshots are taken at instants marked with gray circles in Fig. 8. From left to right, $t=140$, $t=230$, and $t=290$.

lar random 3D component. It would not be strange, then, that a particular section of the whole pipe receives a more effective initial random field and ends up triggering transition ahead of the rest of the sections, which eventually achieve enough energy to also destabilize their region of influence, now probably competing with another mechanism, namely the growth of the already transitioned turbulent patches. For all this, the long pipe could be behaving as the most effective of 5 short pipes, each with a different random noise. This is just a simplification, since the different sections of the long pipe are not evolving independently, but gives an idea of what could be actually happening.

Figure 9 shows the same pictures that were presented in Fig. 5 except those for the largest time at which developed turbulence is observed. The same caption times that were used for the short pipe have been retained, although the 3D perturbation is at slightly different stages of evolution. The fact is that streaks are evolving all throughout the process and, therefore, influencing the location and shape of the 3D perturbation independently of its magnitude, which depends on the pseudolinear inflectional instability mechanism.

The sequence shows a very good agreement between short and long pipe results. Only the smallest scales are slightly worse resolved in the long pipe, as some resolution has been sacrificed to produce a longer domain. It is interesting to see how the transition process is dominated by short-medium wavelengths that get destabilized at random locations along the pipe length, are advected with the mean flow and end up triggering transition. Transition can be considered both local and global in nature. Local, because turbulence first appears at discrete axial positions. Global, because the spacing of these axial positions is considerably short and no intermittent structures such as slugs have time or space to appear and then stretch freely to end up polluting the whole domain.

V. CONCLUSIONS

The capability of vortical streamwise perturbations to trigger transition in pipe flow has been assessed and an upper bound for their critical amplitude provided by means of accurate numerical simulations based on a theoretical scenario of transition that has been proved to be universal in many other shear flows. The computations have been carried out using suitable time windows, making it possible to distinguish relaminarization from long-lasting nonlinear chaotic dynamics. The criteria for transition within the specified time horizons is based on the comparison of relative amplitude of the two-dimensional and three-dimensional perturbation components.

The computed amplitude threshold seems to scale differently for vortical perturbations consisting of different numbers of pairs of rolls. Thus, our best estimates suggest that single-paired vortical disturbances follow an asymptotic scaling law $A_c \sim \mathrm{Re}^{-1.5 \leqslant \gamma \leqslant -1.35}$, while double and triple-paired perturbations respond to scaling laws $A_c \sim \mathrm{Re}^{-1.1}$ and $A_c \sim \mathrm{Re}^{-1.0}$, respectively, for the highest Reynolds numbers explored. Although the critical threshold shrinks faster for the single-paired vortical disturbances, two or three pairs of rolls are more effective in triggering transition within the explored Re range, making it adventurous to proclaim which type of perturbations will dominate at higher Re numbers.

Results at the lower end of the explored Re, where even very strong disturbances only lead to transient destabilization, show evidence of the vertical region of what is often called the *double threshold*. Somewhere around $\mathrm{Re} \sim 2000$, the critical threshold tends to a vertical asymptote and no sustained turbulence is ever achieved for lower Re.

The instability mechanisms based on the streak breakdown process presented in this work may be difficult to reproduce in the laboratory due to the fact that this scenario requires a streamwise initial perturbation, which is irrealizable in experiments by localized injections that necessarily

trigger three-dimensional components of some streamwise structure. In addition, our numerical explorations do not exhibit any of the transitional structures frequently observed in experiments, characterized by the coexistence or intermittency between laminar and turbulent regimes. Further computations carried out for pipe aspect ratio $\Lambda \sim 100$ involving nearly 1.5×10^5 degrees of freedom confirm the global nature of the considered instability mechanism, where long wavelengths take the lead only towards the final stage before transition. Nevertheless, the length scale of these developing waves is not dramatically misrepresented in the short pipe computations.

Other internal mechanisms could also be at work in the transition process and also longer time horizons with $T > T_{\max}$ should be explored in order to check for eventual relaminarization of cases considered turbulent in the present work, along with its implications in the value of the exponent, i.e., $\gamma = \gamma(T)$. All these issues will be addressed in future works but they are currently far beyond the scope of our study.

ACKNOWLEDGMENTS

This work was supported by the Spanish Ministry of Science and Technology, Grant No. FIS2004-01336. The work of F. Mellibovsky was also supported by the UPC-RECERCA doctoral research grant scheme of the Universitat Politècnica de Catalunya.

[1] V. A. Romanov, "Stability of plane-parallel Couette flow," Funct. Anal. Appl. **7**, 137 (1973).
[2] O. Dauchot and F. Daviaud, "Finite amplitude perturbation and spots growth mechanism in plane Couette flow," Phys. Fluids **7**, 335 (1995).
[3] A. Schmiegel and B. Eckhardt, "Fractal stability border in plane Couette flow," Phys. Rev. Lett. **79**, 5250 (1997).
[4] D. Barkley and L. S. Tuckerman, "Computational study of turbulent laminar patterns in Couette flow," Phys. Rev. Lett. **94**, 014502 (2005).
[5] P. G. Drazin, *Introduction to Hydrodynamic Stability, Cambridge Texts in Applied Mathematics* (Cambridge University Press, Cambridge, 2002).
[6] A. Meseguer and L. N. Trefethen, "Linearized pipe flow to Reynolds number 10^7," J. Comput. Phys. **186**, 178 (2003).
[7] P. J. Schmid and D. S. Henningson, Stability and transition in shear flows, No. 142 in *Applied Mathematical Sciences* (Springer-Verlag, New York, 2000).
[8] A. Darbyshire and T. Mullin, "Transition to turbulence in constant-mass-flux pipe flow," J. Fluid Mech. **289**, 83 (1995).
[9] B. Hof, A. Juel, and T. Mullin, "Scaling of the turbulence transition threshold in a pipe," Phys. Rev. Lett. **91**, 244502 (2003).
[10] O. Reynolds, "An experimental investigation of the circumstances which determine whether the motion of water shall be direct or sinuous, and of the law of resistance in parallel channels," Philos. Trans. R. Soc. London **174**, 935 (1883).
[11] P. J. Schmid and D. S. Henningson, "On the role of linear mechanisms in transition to turbulence," Phys. Fluids **6**, 1396 (1994).
[12] A. Meseguer, "Streak breakdown instability in pipe Poiseuille flow," Phys. Fluids **15**, 1203 (2003).
[13] P. J. Schmid and D. S. Henningson, "Optimal energy growth in Hagen-Poiseuille flow," J. Fluid Mech. **277**, 197 (1994).
[14] M. T. Landahl, "A note on an algebraic instability of inviscid parallel shear flows," J. Fluid Mech. **98**, 243 (1980).
[15] S. C. Reddy, P. J. Schmid, J. S. Baggett, and D. S. Henningson, "On stability of streamwise streaks and transition thresholds in plane channel flows," J. Fluid Mech. **365**, 269 (1998).
[16] S. J. Chapman, "Subcritical transition in channel flows," J. Fluid Mech. **451**, 35 (2002).
[17] M. Nagata, "Three-dimensional finite-amplitude solutions in plane Couette flow: Bifurcation from infinity," J. Fluid Mech. **217**, 519 (1990).
[18] A. Cherhabili and U. Ehrenstein, "Finite-amplitude equilibrium states in plane Couette flow," J. Fluid Mech. **342**, 159 (1997).
[19] A. Schmiegel, "Transition to turbulence in linearly stable shear flows," Ph.D. thesis, Philipps-Universität Marburg (1999).
[20] H. Faisst and B. Eckhardt, "Travelling waves in pipe flow," Phys. Rev. Lett. **91**, 224502 (2003).
[21] H. Wedin and R. R. Kerswell, "Exact coherent structures in pipe flow: travelling wave solutions," J. Fluid Mech. **508**, 333 (2004).
[22] H. Faisst, "Turbulence transition in pipe flow," Ph.D., thesis, Philipps-Universität Marburg (2003).
[23] A. T. Patera and S. A. Orszag, "Finite amplitude stability of axysimmetric pipe flow," J. Fluid Mech. **112**, 467 (1981).
[24] L. N. Trefethen, S. J. Chapman, D. S. Henningson, A. Meseguer, T. Mullin, and F. T. M. Nieuwstadt, "Threshold amplitudes for transition to turbulence in a pipe," Technical Report No. 00/17, Oxford University Computer Laboratory (2000).
[25] D. Hof, C. W. H. van Doorne, J. Westerweel, F. T. M. Nieuwstadt, H. Faisst, B. Eckhardt, H. Wedin, R. R. Kerswell, and F. Waleffe, "Experimental observation of nonlinear travelling waves in turbulent pipe flow," Science **305**, 1594 (2004).
[26] A. Meseguer and L. N. Trefethen, "A spectral Petrov-Galerkin formulation for pipe flow I: Linear stability and transient growth," Technical Report No. 00/18, Oxford University Computer Laboratory (2000).
[27] A. Meseguer and L. N. Trefethen, "A spectral Petrov-Galerkin formulation for pipe flow II: Nonlinear transitional stages," Technical Report No. 01/19, Oxford University Computer Laboratory (2001).
[28] O. Y. Zikanov, "On the instability of pipe Poiseuille flow," Phys. Fluids **8**, 2923 (1996).
[29] H. Shan, B. Ma, Z. Zhang, and F. T. M. Nieuwstadt, "Direct numerical simulation of a puff and a slug in transitional cylindrical pipe flow," JFMA **387**, 39 (1998).